Research Article | Vol. 8, No. 7 | 1 Jul 2017 | BIOMEDICAL OPTICS EXPRESS 3213
Biomedical Optics EXPRESS

# Multiphoton in vivo imaging with a femtosecond semiconductor disk laser

FABIAN F. VOIGT,[1,2,4,6] FLORIAN EMAURY,[3,4,5] PHILIPP BETHGE,[1] DOMINIK WALDBURGER,[3] SANDRO M. LINK,[3] STEFANO CARTA,[1] ALEXANDER VAN DER BOURG,[1] FRITJOF HELMCHEN,[1,2] AND URSULA KELLER[3]

[1]*Laboratory of Neural Circuit Dynamics, Brain Research Institute, University of Zurich, 8057 Zürich, Switzerland*
[2]*Neuroscience Center Zurich, University of Zurich & ETH Zurich, 8057 Zürich, Switzerland*
[3]*Department of Physics, Institute for Quantum Electronics, ETH Zurich, 8093 Zürich, Switzerland*
[4]*These authors have contributed equally*
[5]*emaury@phys.ethz.ch*
[6]*voigt@hifo.uzh.ch*

**Abstract:** We use an ultrafast diode-pumped semiconductor disk laser (SDL) to demonstrate several applications in multiphoton microscopy. The ultrafast SDL is based on an optically pumped Vertical External Cavity Surface Emitting Laser (VECSEL) passively mode-locked with a semiconductor saturable absorber mirror (SESAM) and generates 170-fs pulses at a center wavelength of 1027 nm with a repetition rate of 1.63 GHz. We demonstrate the suitability of this laser for structural and functional multiphoton *in vivo* imaging in both *Drosophila* larvae and mice for a variety of fluorophores (including mKate2, tdTomato, Texas Red, OGB-1, and R-CaMP1.07) and for endogenous second-harmonic generation in muscle cell sarcomeres. We can demonstrate equivalent signal levels compared to a standard 80-MHz Ti:Sapphire laser when we increase the average power by a factor of 4.5 as predicted by theory. In addition, we compare the bleaching properties of both laser systems in fixed Drosophila larvae and find similar bleaching kinetics despite the large difference in pulse repetition rates. Our results highlight the great potential of ultrafast diode-pumped SDLs for creating a cost-efficient and compact alternative light source compared to standard Ti:Sapphire lasers for multiphoton imaging.



**OCIS codes:** (180.4315) Nonlinear microscopy; (180.2520) Fluorescence microscopy; (170.3880) Medical and biological imaging; (140.4050) Mode-locked lasers; (140.5960) Semiconductor lasers.

## References and links

1. F. Helmchen and W. Denk, "Deep tissue two-photon microscopy," Nat. Methods **2**(12), 932–940 (2005).
2. W. R. Zipfel, R. M. Williams, and W. W. Webb, "Nonlinear magic: multiphoton microscopy in the biosciences," Nat. Biotechnol. **21**(11), 1369–1377 (2003).
3. W. Denk, J. H. Strickler, and W. W. Webb, "Two-photon laser scanning fluorescence microscopy," Science **248**(4951), 73–76 (1990).
4. I. Freund and M. Deutsch, "Second-harmonic microscopy of biological tissue," Opt. Lett. **11**(2), 94–96 (1986).
5. A. Miyawaki and Y. Niino, "Molecular Spies for Bioimaging--Fluorescent Protein-Based Probes," Mol. Cell **58**(4), 632–643 (2015).
6. B. A. Wilt, L. D. Burns, E. T. Wei Ho, K. K. Ghosh, E. A. Mukamel, and M. J. Schnitzer, "Advances in Light Microscopy for Neuroscience," Annu. Rev. Neurosci. **32**(1), 435–506 (2009).
7. C. Wang, R. Liu, D. E. Milkie, W. Sun, Z. Tan, A. Kerlin, T. W. Chen, D. S. Kim, and N. Ji, "Multiplexed aberration measurement for deep tissue imaging in vivo," Nat. Methods **11**(10), 1037–1040 (2014).
8. M. Drobizhev, N. S. Makarov, S. E. Tillo, T. E. Hughes, and A. Rebane, "Two-photon absorption properties of fluorescent proteins," Nat. Methods **8**(5), 393–399 (2011).
9. B. W. Tilma, M. Mangold, C. A. Zaugg, S. M. Link, D. Waldburger, A. Klenner, A. S. Mayer, E. Gini, M. Golling, and U. Keller, "Recent advances in ultrafast semiconductor disk lasers," Light Sci. Appl. **4**(7), e310 (2015).
10. M. A. Gaafar, A. Rahimi-Iman, K. A. Fedorova, W. Stolz, E. U. Rafailov, and M. Koch, "Mode-locked semiconductor disk lasers," Adv. Opt. Photonics **8**(3), 370–400 (2016).

#291630 https://doi.org/10.1364/BOE.8.003213
Journal © 2017 Received 28 Mar 2017; revised 30 May 2017; accepted 30 May 2017; published 13 Jun 2017

Biomedical Optics EXPRESS


11 S. Tang, T. B. Krasieva, Z. Chen, G. Tempea, and B. J. Tromberg, "Effect of pulse duration on two-photon excited fluorescence and second harmonic generation in nonlinear optical microscopy," J. Biomed. Opt. **11**, 020501 (2006).
12. B. E. A. Saleh and M. C. Teich, *Fundamentals of photonics,* 2nd ed., Wiley series in pure and applied optics (Wiley Interscience, Hoboken, N.J., 2007), pp. xix, 1175 p.
13. A. Hopt and E. Neher, "Highly Nonlinear Photodamage in Two-Photon Fluorescence Microscopy," Biophys. J. **80**(4), 2029–2036 (2001).
14. P. G. Antal and R. Szipőcs, "Tunable, low-repetition-rate, cost-efficient femtosecond Ti:sapphire laser for nonlinear microscopy," Appl. Phys. B **107**(1), 17–22 (2012).
15. C. G. Durfee, T. Storz, J. Garlick, S. Hill, J. A. Squier, M. Kirchner, G. Taft, K. Shea, H. Kapteyn, M. Murnane, and S. Backus, "Direct diode-pumped Kerr-lens mode-locked Ti:sapphire laser," Opt. Express **20**(13), 13677–13683 (2012).
16. K. Gürel, V. J. Wittwer, M. Hoffmann, C. J. Saraceno, S. Hakobyan, B. Resan, A. Rohrbacher, K. Weingarten, S. Schilt, and T. Südmeyer, "Green-diode-pumped femtosecond Ti:Sapphire laser with up to 450 mW average power," Opt. Express **23**(23), 30043–30048 (2015).
17. M. D. Young, S. Backus, C. Durfee, and J. Squier, "Multiphoton imaging with a direct-diode pumped femtosecond Ti:sapphire laser," J. Microsc. **249**(2), 83–86 (2013).
18 S. Tang, J. Liu, T. B. Krasieva, Z. Chen, and B. J. Tromberg, "Developing compact multiphoton systems using femtosecond fiber lasers," J. Biomed. Opt. **14**, 030508 (2009).
19. E. P. Perillo, J. E. McCracken, D. C. Fernée, J. R. Goldak, F. A. Medina, D. R. Miller, H.-C. Yeh, and A. K. Dunn, "Deep in vivo two-photon microscopy with a low cost custom built mode-locked 1060 nm fiber laser," Biomed. Opt. Express **7**(2), 324–334 (2016).
20. K. E. Sheetz, E. E. Hoover, R. Carriles, D. Kleinfeld, and J. A. Squier, "Advancing multifocal nonlinear microscopy: development and application of a novel multibeam Yb:KGd(WO4)2 oscillator," Opt. Express **16**(22), 17574–17584 (2008).
21. K. Svoboda, W. H. Knox, S. Tsuda, and W. Denk, "Two-photon-excitation scanning microscopy of living neurons with a saturable Bragg reflector mode-locked diode-pumped Cr:LiSrAlFl laser," Opt. Lett. **21**(17), 1411–1413 (1996).
22. A. Robertson, R. Knappe, and R. Wallenstein, "Kerr-lens modelocked Cr:LiSAF femtosecond laser pumped by diffraction-limited output of a 672-nm diode-laser master-oscillator power-amplifier system," J. Opt. Soc. Am. B **14**(3), 672–675 (1997).
23. S.-W. Chu, I. H. Chen, T.-M. Liu, P. C. Chen, C.-K. Sun, and B.-L. Lin, "Multimodal nonlinear spectral microscopy based on a femtosecond Cr:forsterite laser," Opt. Lett. **26**(23), 1909–1911 (2001).
24. T.-M. Liu, S.-W. Chu, C.-K. Sun, B.-L. Lin, P.-C. Cheng, and I. Johnson, "Multiphoton confocal microscopy using a femtosecond Cr:forsterite laser," Scanning **23**(4), 249–254 (2001).
25. B. Resan, R. Aviles-Espinosa, S. Kurmulis, J. Licea-Rodriguez, F. Brunner, A. Rohrbacher, D. Artigas, P. Loza-Alvarez, and K. J. Weingarten, "Two-photon fluorescence imaging with 30 fs laser system tunable around 1 micron," Opt. Express **22**(13), 16456–16461 (2014).
26. M. Kuznetsov, "VECSEL Semiconductor Lasers: A Path to High-Power, Quality Beam and UV to IR Wavelength by Design," in *Semiconductor Disk Lasers*, O. G. Okhotnikov, ed. (Wiley-VCH Verlag GmbH & Co. KGaA, 2010), pp. 1–71.
27. H. Yokoyama, H. Guo, T. Yoda, K. Takashima, K. Sato, H. Taniguchi, and H. Ito, "Two-photon bioimaging with picosecond optical pulses from a semiconductor laser," Opt. Express **14**(8), 3467–3471 (2006).
28. M. Kuramoto, N. Kitajima, H. Guo, Y. Furushima, M. Ikeda, and H. Yokoyama, "Two-photon fluorescence bioimaging with an all-semiconductor laser picosecond pulse source," Opt. Lett. **32**(18), 2726–2728 (2007).
29. H. Wang, L. Kong, A. Forrest, D. Bajek, S. E. Haggett, X. Wang, B. Cui, J. Pan, Y. Ding, and M. A. Cataluna, "Ultrashort pulse generation by semiconductor mode-locked lasers at 760 nm," Opt. Express **22**(21), 25940–25946 (2014).
30. Y. Kusama, Y. Tanushi, M. Yokoyama, R. Kawakami, T. Hibi, Y. Kozawa, T. Nemoto, S. Sato, and H. Yokoyama, "7-ps optical pulse generation from a 1064-nm gain-switched laser diode and its application for two-photon microscopy," Opt. Express **22**(5), 5746–5753 (2014).
31. M. Mangold, S. M. Link, A. Klenner, C. A. Zaugg, M. Golling, B. W. Tilma, and U. Keller, "Amplitude noise and timing jitter characterization of a high-power Mode-Locked Integrated External-Cavity Surface Emitting Laser," IEEE Photonics J. **6**(1), 1–9 (2014).
32. A. Giesen, H. Hügel, A. Voss, K. Wittig, U. Brauch, and H. Opower, "Scalable Concept for Diode-Pumped High-Power Solid-State Lasers," Appl. Phys. B **58**(5), 365–372 (1994).
33. R. Michalzik, "VCSELs: A Research Review," in *VCSELs: Fundamentals, Technology and Applications of Vertical-Cavity Surface-Emitting Lasers*, R. Michalzik, ed. (Springer Berlin Heidelberg, Berlin, Heidelberg, 2013), pp. 3–18.
34. S. Hoogland, S. Dhanjal, A. C. Tropper, J. S. Roberts, R. Haring, R. Paschotta, F. Morier-Genoud, and U. Keller, "Passively mode-locked diode-pumped surface-emitting semiconductor laser," IEEE Photonics Technol. Lett. **12**(9), 1135–1137 (2000).
35. U. Keller and A. C. Tropper, "Passively modelocked surface-emitting semiconductor lasers," Phys. Rep. **429**(2), 67–120 (2006).

Biomedical Optics EXPRESS


36. R. Häring, R. Paschotta, E. Gini, F. Morier-Genoud, D. Martin, H. Melchior, and U. Keller, "Picosecond surface-emitting semiconductor laser with >200 mW average power," Electron. Lett. **37**(12), 766–767 (2001).
37. A. Garnache, S. Hoogland, A. C. Tropper, I. Sagnes, G. Saint-Girons, and J. S. Roberts, "Sub-500-fs soliton pulse in a passively mode-locked broadband surface-emitting laser with 100-mW average power," Appl. Phys. Lett. **80**(21), 3892–3894 (2002).
38. S. Hoogland, A. Garnache, I. Sagnes, J. S. Roberts, and A. C. Tropper, "10-GHz Train of Sub-500-fs Optical Soliton-Like Pulses From a Surface-Emitting Semiconductor Laser," IEEE Photonics Technol. Lett. **17**(2), 267–269 (2005).
39. K. G. Wilcox, A. H. Quarterman, H. Beere, D. A. Ritchie, and A. C. Tropper, "High Peak Power Femtosecond Pulse Passively Mode-Locked Vertical-External-Cavity Surface-Emitting Laser," IEEE Photonics Technol. Lett. **22**(14), 1021–1023 (2010).
40. P. Klopp, U. Griebner, M. Zorn, and M. Weyers, "Pulse repetition rate up to 92 GHz or pulse duration shorter than 110 fs from a mode-locked semiconductor disk laser," Appl. Phys. Lett. **98**(7), 071103 (2011).
41. C. A. Zaugg, A. Klenner, M. Mangold, A. S. Mayer, S. M. Link, F. Emaury, M. Golling, E. Gini, C. J. Saraceno, B. W. Tilma, and U. Keller, "Gigahertz self-referenceable frequency comb from a semiconductor disk laser," Opt. Express **22**(13), 16445–16455 (2014).
42. D. Waldburger, S. M. Link, M. Mangold, C. G. E. Alfieri, E. Gini, M. Golling, B. W. Tilma, and U. Keller, "High-power 100 fs semiconductor disk lasers," Optica **3**(8), 844–852 (2016).
43 J. M. Girkin and D. L. Wokosin, "Novel compact sources for multiphoton microscopy," Proc. SPIE Multiphoton Microscopy in the Biomedical Sciences **4262**, 186 (2001).
44. R. Aviles-Espinosa, G. Filippidis, C. Hamilton, G. Malcolm, K. J. Weingarten, T. Südmeyer, Y. Barbarin, U. Keller, S. I. C. O. Santos, D. Artigas, and P. Loza-Alvarez, "Compact ultrafast semiconductor disk laser: targeting GFP based nonlinear applications in living organisms," Biomed. Opt. Express **2**(4), 739–747 (2011).
45. K. G. Wilcox, A. C. Tropper, H. E. Beere, D. A. Ritchie, B. Kunert, B. Heinen, and W. Stolz, "4.35 kW peak power femtosecond pulse mode-locked VECSEL for supercontinuum generation," Opt. Express **21**(2), 1599–1605 (2013).
46. S. Mirkhanov, A. H. Quarterman, S. Swift, B. B. Praveen, C. J. C. Smyth, and K. G. Wilcox, "Multiphoton imaging with high peak power VECSELs," Proc. SPIE Vertical External Cavity Surface Emitting Lasers **9734**, 973412 (2016)
47 K. Podgorski and G. N. Ranganathan, "Brain heating induced by near infrared lasers during multi-photon microscopy," J. Neurophysiol **116**(3) 1012-1023 (2016).
48. N. Ji, J. C. Magee, and E. Betzig, "High-speed, low-photodamage nonlinear imaging using passive pulse splitters," Nat. Methods **5**(2), 197–202 (2008).
49. S.-W. Chu, T.-M. Liu, C.-K. Sun, C.-Y. Lin, and H.-J. Tsai, "Real-time second-harmonic-generation microscopy based on a 2-GHz repetition rate Ti:sapphire laser," Opt. Express **11**(8), 933–938 (2003).
50. A. Ehlers, I. Riemann, S. Martin, R. Le Harzic, A. Bartels, C. Janke, and K. König, "High (1 GHz) repetition rate compact femtosecond laser: A powerful multiphoton tool for nanomedicine and nanobiotechnology," J. Appl. Phys. **102**(1), 014701 (2007).
51 H. Studier, H. G. Breunig, and K. König, "Two-photon imaging with 80 MHz and 1-GHz repetition rate Ti:sapphire oscillators," Proc. SPIE Multiphoton Microscopy in the Biomedical Sciences X **7569** (2010).
52. H. Studier, H. G. Breunig, and K. König, "Comparison of broadband and ultrabroadband pulses at MHz and GHz pulse-repetition rates for nonlinear femtosecond-laser scanning microscopy," J. Biophotonics **4**(1), 84–91 (2011).
53. J. L. Chen, F. F. Voigt, M. Javadzadeh, R. Krueppel, and F. Helmchen, "Long-range population dynamics of anatomically defined neocortical networks," eLife **5**, 14679 (2016).
54 F. F. Voigt, J. L. Chen, R. Krueppel, and F. Helmchen, "A modular two-photon microscope for simultaneous imaging of distant cortical areas in vivo," Proc. SPIE Multiphoton Microscopy in the Biomedical Sciences XV **93292**, 93292 (2015).
55. M. Mangold, M. Golling, E. Gini, B. W. Tilma, and U. Keller, "Sub-300-femtosecond operation from a MIXSEL," Opt. Express **23**(17), 22043–22059 (2015).
56. S. Caviglia, M. Brankatschk, E. J. Fischer, S. Eaton, and S. Luschnig, "Staccato/Unc-13-4 controls secretory lysosome-mediated lumen fusion during epithelial tube anastomosis," Nat. Cell Biol. **18**(7), 727–739 (2016).
57. D. Kleinfeld, P. P. Mitra, F. Helmchen, and W. Denk, "Fluctuations and stimulus-induced changes in blood flow observed in individual capillaries in layers 2 through 4 of rat neocortex," Proc. Natl. Acad. Sci. U.S.A. **95**(26), 15741–15746 (1998).
58. C. Grienberger and A. Konnerth, "Imaging Calcium in Neurons," Neuron **73**(5), 862–885 (2012).
59. J. Schindelin, I. Arganda-Carreras, E. Frise, V. Kaynig, M. Longair, T. Pietzsch, S. Preibisch, C. Rueden, S. Saalfeld, B. Schmid, J. Y. Tinevez, D. J. White, V. Hartenstein, K. Eliceiri, P. Tomancak, and A. Cardona, "Fiji: an open-source platform for biological-image analysis," Nat. Methods **9**(7), 676–682 (2012).
60. G.-A. Pilz, S. Carta, A. Stäuble, A. Ayaz, S. Jessberger, and F. Helmchen, "Functional Imaging of Dentate Granule Cells in the Adult Mouse Hippocampus," J. Neurosci. **36**(28), 7407–7414 (2016).
61. C. Stosiek, O. Garaschuk, K. Holthoff, and A. Konnerth, "In vivo two-photon calcium imaging of neuronal networks," Proc. Natl. Acad. Sci. U.S.A. **100**(12), 7319–7324 (2003).

Biomedical Optics EXPRESS

62. P. Golshani, J. T. Gonçalves, S. Khoshkhoo, R. Mostany, S. Smirnakis, and C. Portera-Cailliau, "Internally mediated developmental desynchronization of neocortical network activity," J. Neurosci. **29**(35), 10890–10899 (2009).
63. X. Chen, U. Leischner, N. L. Rochefort, I. Nelken, and A. Konnerth, "Functional mapping of single spines in cortical neurons in vivo," Nature **475**(7357), 501–505 (2011).

## 1. Introduction

Over the past decades, multiphoton microscopy (MPM) methods have been widely adopted in biomedical research owing to their combination of high spatial resolution, intrinsic optical sectioning and the ability to perform deep imaging in scattering samples [1, 2]. Nonlinear imaging techniques such as two-photon microscopy [3], second-harmonic generation (SHG) [4], and nonlinear Raman microscopy offer a wide variety of label-dependent and label-free contrast mechanisms to study fixed and living tissues. While imaging capabilities are constantly improving with the introduction of new labeling methods [5] and novel scanning approaches [6], the cost of such microscopes is still prohibitively high for many laboratories. A considerable fraction of the budget for a multiphoton system has to be allocated to acquire an expensive ultrafast laser source such as a tunable Ti:Sapphire laser. Typical commercial Ti:Sapphire lasers acquired for this application generate ≈1.5 to 3.5 W of average power at the gain maximum of around 800 nm. However, for most experiments, only a small fraction is used to illuminate a biological sample. For example, when imaging the superficial layers of the murine neocortex with a single scanned excitation spot, an average power between 10 mW (for superficial layer 2/3) and 100 mW (for deep layer 5) is sufficient for functional recordings with the calcium indicator GCaMP6 [7]. As the transmittance of the microscope's optical path can be optimized to >50%, considerable potential exists for less expensive laser sources with a few hundreds of mW output power and with a center wavelength close to the absorption peak of selected fluorophores (Fig. 1).

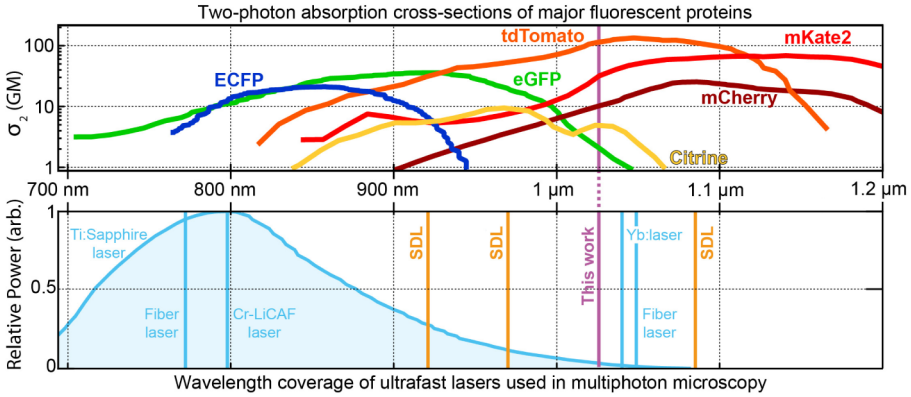


Fig. 1. Overview of the two-photon absorption cross-sections of various fluorescent proteins [8] used in two-photon microscopy combined with the spectral coverage of existing ultrafast lasers. Ti:Sapphire lasers have a large tuning range of >300 nm. In contrast, other commercial ultrafast lasers (blue lines) cannot be tuned to match the absorption peaks of dyes. Ultrafast semiconductor disk lasers (SDLs, orange lines) have the potential to become less expensive sources and can be designed with emission wavelengths between 650 and 2800 nm (typical lasers with a center wavelength at 920-nm, 970-nm and 1080-nm are shown here, but more options are possible) [9, 10]. The SDL laser presented in this paper operates at 1027 nm (indicated as "This work").

An ideal ultrafast laser for MPM should be able to efficiently excite a variety of fluorophores, generate sufficiently short pulses, and provide good beam quality. In addition, a small footprint to ease integration into a microscope system, maintenance-free operation, and an affordable price are highly beneficial. The pulse duration $\tau$ needs to be optimized as there is a trade-off between the generated two-photon signal which scales theoretically as $\tau^{-1}$

Biomedical Optics EXPRESS

(experimentally $\tau^{-0.85}$) [11], the pulse broadening which scales as $\tau^{-1}$ [12], and the photo-damage effects which scales as $\tau^{1.5}$ [13]. In practice, most imaging studies use a pulse duration in the range of 100-200 fs as a compromise.

Recently, Ti:Sapphire laser technology was improved towards higher efficiency [14] and by novel direct-diode pumping schemes using high-power visible semiconductor lasers [15, 16]. Such a Ti:Sapphire laser was demonstrated to be a suitable source for MPM [17] but despite the lower cost and improvements in compactness, commercial impact is still limited. Fiber lasers [18, 19], Yb:$KGd(WO_4)_2$ [20], Cr:LiSrAlFl [21] or Cr:LiSAF [22] crystals in a bulk configuration, or Cr:Forsterite lasers operating at 1230 nm [23, 24] are interesting low-cost alternatives in MPM applications. However, the center wavelengths of these lasers limit their operation to only a few discrete spectral regions. Access to a wider spectrum can be obtained by spectral broadening with a tunable cavity [25], but at the expense of a significant increase in complexity for the laser source.

Semiconductor lasers are attractive for biological applications as the center wavelength can be optimized towards desired values by bandgap engineering. In microscopy, this approach has already been commercialized successfully for continuous-wave (cw) lasers, with a wide available range of optically pumped semiconductor lasers at center wavelengths ranging from the UV to the mid-IR (Fig. 1.12 in [26]). During the past decades various concepts for pulsed semiconductor lasers suitable for MPM were demonstrated, such as gain-switched semiconductor lasers [27], external cavity mode-locked laser diodes [28, 29], or mode-locked laser diodes [30]. These pulsed lasers, however, all rely on transverse emitters and in most cases on an additional amplifier, producing rather long pulses in the 1-20 ps range with rather poor beam quality. This requires higher average power when used in nonlinear microscopy. In contrast, a surface emitting semiconductor laser provides an ideal Gaussian beam and optical pumping allows for power scaling. The interaction with the gain medium is perpendicular to the gain layers and much shorter than the cavity length which leads to excellent noise performance [31]. In analogy to solid-state thin-disk lasers, this type of laser is also referred to as semiconductor disk laser (SDL) [32].

Mode-locked SDLs combine simple cavity design, excellent beam quality, and scalability of the production process. The laser cavity can be embedded directly on the semiconductor chip creating a Vertical Cavity Surface Emitting Laser (VCSEL), which is employed in lighting and telecommunications [33]. With electrical or optical pumping [33] high output powers can be achieved directly from the oscillator. A vertically emitting semiconductor chip with an external cavity leads to a Vertical External Cavity Surface Emitting Laser (VECSEL; Fig. 2(A)), yielding better beam quality ($M^2 < 1.05$ in both axes) and higher power compared to VCSELs. Moreover, this approach allows for an intracavity semiconductor saturable absorber mirror (SESAM) for passive pulse formation [9, 34, 35] (Fig. 2(A)). Since the first demonstration of a SESAM-mode-locked VECSEL in 2000 [34], the laser performance has been drastically improved. Mode-locked VECSELs have been operated from 650 nm to 2800 nm [9, 10], with the best results achieved in the 900-1100 nm region due to lattice-matched materials for high-quality distributed Bragg reflectors (DBRs) and due to low-cost high-power pump diode arrays operating at 808 nm.

Biomedical Optics EXPRESS

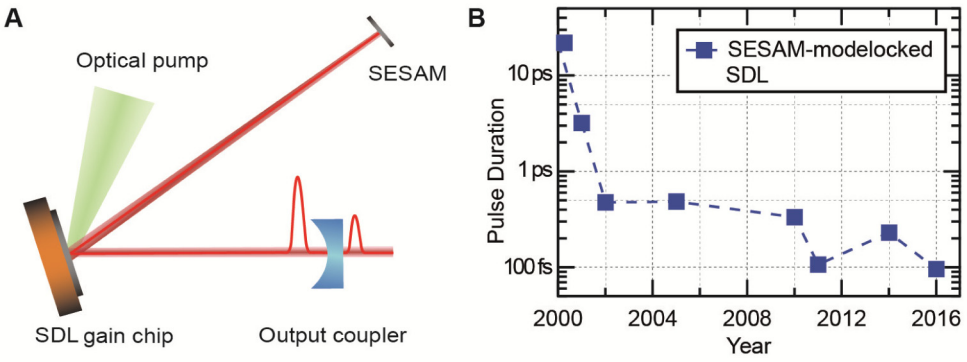


Fig. 2. A) Typical laser cavity of a pulsed Semiconductor Disk Laser (SDL) or Vertical External Cavity Surface Emitting Laser (VECSEL) consisting of an optically pumped gain chip, a SESAM to enable pulse formation with passive mode-locking and an output coupler. The cavity length is set to reach a pulse repetition rate of ≈1-2 GHz with an (unfolded) length of 10-15 cm. B) Overview of the evolution of pulse durations from SESAM-mode-locked SDLs around 1000 nm since the first demonstration in 2000 [34, 36–41], recently reaching sub-100 fs [42].

Figure 2(B) illustrates the evolution of the shortest pulse durations of fundamental SESAM-mode-locked VECSELs operating around 1000 nm during the last two decades [34, 36–42]. While several other mode-locking techniques were demonstrated [31, 32], SESAM-mode-locked VECSELs are currently the most promising approach to reach shorter pulses with the important milestone of sub-100 fs achieved in 2016 [42]. The use of a SDL for MPM was first proposed by Girkin and Wokosin in 2001 [43], who also noted that an array of SDLs operating at different wavelengths might constitute a cost-efficient replacement of a tunable Ti:Sapphire source. In 2011, a pulsed SDL was used for MPM for the first time [44]. This laser operated at 500 MHz with 1.5-ps long pulses at a center wavelength of 965 nm and an average output power of 287 mW. It allowed imaging of neuronal processes and cell bodies in *Caenorhabditis elegans* (*C. elegans*) expressing Green Fluorescent Protein (GFP). While this first demonstration showed the potential of ultrafast SDLs, the long pulses limited the practical use of such a laser compared to existing technology. In 2013, a VECSEL with a peak power of 4.35 kW [45] and a pulse duration of 450 fs was developed and foreseen to be applicable for MPM [46]. With the recent progress in the laser technology [42], the pulse length of ultrafast SDLs has become more comparable with Ti:Sapphire lasers commonly used for MPM.

In this paper, we demonstrate the use of the latest generation of mode-locked SDLs for a variety of MPM imaging applications. We describe the microscope setup and a novel ultrafast SDL that generated pulses as short as ≈100 fs [42] and 145 mW of average power. At a center wavelength of 1027 nm, our laser delivers 72 mW of average power and 170 fs pulses below the objective. We compare the two-photon excited fluorescence signal and bleaching dynamics generated with the SDL to data recorded from the same samples with a standard Ti:Sapphire laser. We then proceed to present a number of *in vivo* imaging demonstrations, ranging from two-photon and SHG imaging in *Drosophila* larvae to structural and functional imaging in the living mouse brain using acute or chronic cranial window preparations. With this work, we demonstrate for the first time — to the best of our knowledge — that a state-of-the art femtosecond SDL is a compelling laser source for MPM applications in neuroscience and biology in general. Given the lower complexity and thus lower cost of SDLs compared to Ti:Sapphire lasers, we believe that SDLs will pave the way towards a wider adoption of MPM in research and medical applications.

Biomedical Optics EXPRESS

## 2. Multiphoton imaging at high laser repetition rates

As noted by Girkin and Wokosin [43], due to the short gain carrier lifetime in semiconductors passively mode-locked SDLs typically operate at repetition rates in the gigahertz domain compared to the approximately 80-MHz repetition rate provided by Ti:Sapphire lasers. As the two-photon fluorescence signal scales as $S \propto P_{avg}^2/(\tau \cdot f_{rep})$ [3], increasing the repetition rate $f_{rep}$ n-fold requires scaling the average excitation power $P_{avg}$ by $n^{1/2}$ in order to keep the emitted fluorescence signal constant (see Fig. 3).

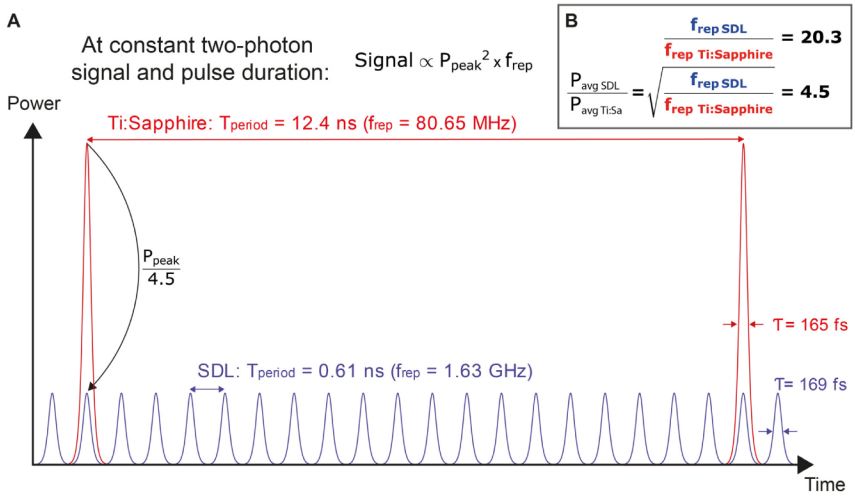


Fig. 3. Multiphoton microscopy (MPM) imaging at high repetition rates: A) Overlay of the pulse trains from a Ti:Sapphire laser and a SDL set to generate the same two-photon excited fluorescence signal at comparable pulse duration, center wavelength, and optical resolution. We use the parameters of the two lasers compared in this study as examples. B) In order to achieve constant signal, the ratio of average powers has to be set to the square root of the ratio of repetition rates.

High average power may lead to heating-induced damage of the sample, which has to be prevented for imaging in living tissue. Especially during functional imaging in the mouse brain [47], power levels have to be closely monitored. In contrast to heating due to linear absorption, photodamage in two-photon microscopy has been reported to scale as $D \propto P_{avg}^{\beta}$ with $\beta > 2$ [13]. This strong nonlinear dependence may reduce photobleaching rates at high repetition rates as demonstrated by Ji et al. [48] through the use of passive pulse-splitting. In reference [48], the authors divided pulses from a standard 80 MHz Ti:Sapphire laser into bursts of pulses of smaller peak power, adding, however, the complexity and cost of the custom beamsplitting setup to the one of the laser. The use of GHz sources based on Ti:Sapphire as a gain medium has been demonstrated in only a small number of studies for SHG microscopy [49] and two-photon microscopy [50–52], likely due to the high complexity and cost of these lasers.

## 3. Experimental setup: lasers and microscope

This section describes the details of the microscope setup and the parameters of the SDL and Ti:Sapphire laser used in this study.

### *3.1 The microscope setup*

The multiphoton microscope used in this study is based on a multi-area two-photon microscope described previously (Fig. 4) [53, 54]. Excitation light from either the SDL (see section 3.3) or a Ti:Sapphire laser (Spectra-Physics Mai Tai HP DS; see section 3.4) was intensity-modulated with Pockels cells (Conoptics 350-105 for the SDL and Conoptics

Biomedical Optics EXPRESS

350-80 for the Ti:Sapphire laser) and the laser beam expanded before being sent to the scan mirrors (6220H, d = 10 mm, Cambridge Technologies). The beam then passed a telescope formed by a f = 89 mm scan lens (S4LFT0089, Sill Optics) and a f = 200 mm tube lens (AC508-200B, Thorlabs) and was directed into the microscope objective (Olympus XLUMPlanFL 20x 0.95W or a Nikon CFI75 LWD 16xW NA 0.8).

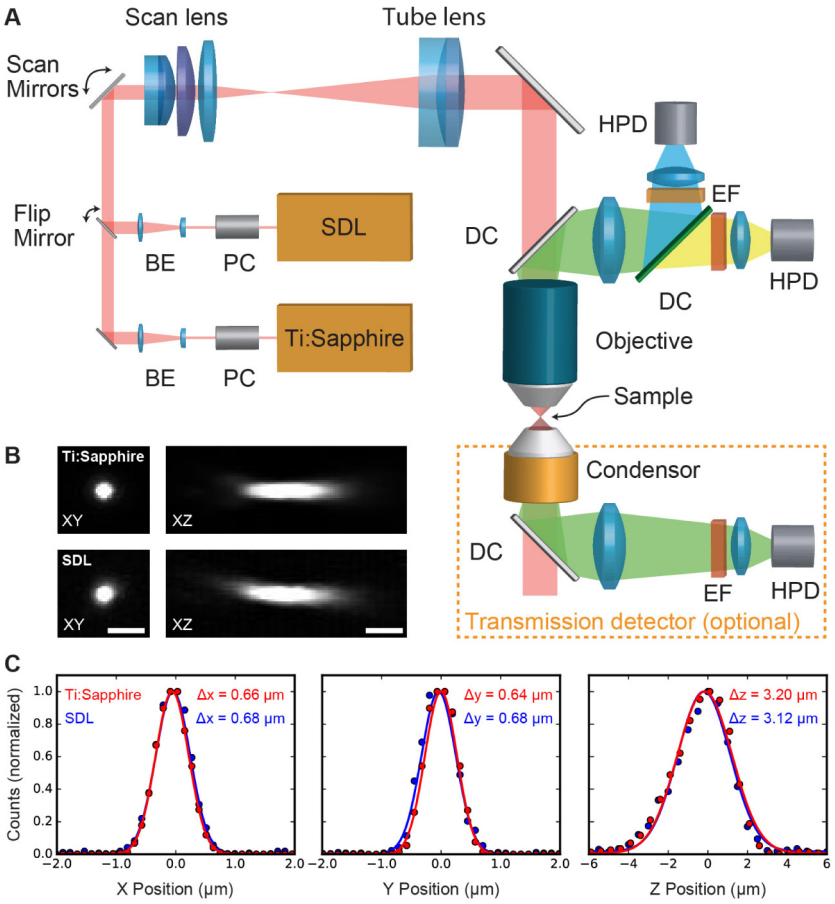


Fig. 4. A) Overview of the microscope setup: Excitation light from either the SDL or a Ti:Sapphire laser (Spectra-Physics Mai Tai DeepSee) can be coupled into the microscope via a Pockels cell (PC) and a beam expander (BE). After the scan mirrors, the beam is directed into the objective by a scan and tube lens. The emission light is sent to a two-channel detection system via dichroic mirrors (DCs), emission filters (EF) and then collected by hybrid photo-detectors (HPDs). For small, transparent samples, a transmission detector with a single HPD can be added. B) Maximum intensity projections of images of the same 200 nm bead taken with the Ti:Sapphire and SDL. C) Gaussian fit of the data in B) with full width at half maximum (FWHM) values for both lasers.

For detection, the emitted light was separated from the excitation light by an IR-VIS dichroic (HC705 MP Longpass, AHF AG) and directed towards hybrid photodetectors (HPD, R11322U-40 MOD, Hamamatsu). For small transparent samples a custom single-channel transmission detector, composed of a NA = 1.0 water immersion condenser (Zeiss) and including an additional HPD, could be placed below the sample. HPD signals were preamplified (C1077B, Hamamatsu) and digitized by an analog-to-digital converter (ADC, NI-5771, National Instruments) connected to a field-programmable array (FPGA, NI-7962R, National Instruments). Scanning and data acquisition were controlled using the two-photon microscope control software “Scope”, (rkscope.sourceforge.net). For SHG imaging, a 514/30

Biomedical Optics EXPRESS

BrightLine HC (AHF AG) emission filter was used both in the transmission and reflection path. In the epidetection path, a dichroic mirror with a cut-on wavelength of 552 nm (HC BS 552, AHF AG) was used to separate the SHG emission from longer-wavelength fluorescence. For parallel fluorescence imaging with a red and green channel (e.g. Figure 11), a filter set consisting of a Qioptic DC-Green dichroic and two emission filters (Semrock Brightline Basic 535/22 and Chroma ET605/70M) were used.

### *3.2 Matching of point spread functions between the SDL and the Ti:Sapphire laser*

In order to ensure that both lasers were focused equally well for the comparison experiments, we matched the point spread functions (PSFs) of the microscope for the two lasers. For this, we adapted the beam expansion optics in front of both lasers to equalize the beam diameters at the 20x objective. To allow maximum power throughput, we underfilled the back aperture of the 20x objective, which means that the PSFs were not diffraction-limited for NA = 0.95 at 1027 nm (Figs. 4(B) and (C)). PSF measurements were done using Fluoresbrite Multifluorescent Microspheres (Polyscience, 0.2 µm). For the SDL, we measured a full width at half maximum of the PSF of $FWHM_x$ = 0.68 ± 0.01 µm, $FWHM_y$ = 0.68 ± 0.02 µm, and $FWHM_z$ = 3.14 ± 0.01 µm ( ± SEM, n = 3 beads), demonstrating in addition the good beam quality of the SDL. For the Ti:Sapphire laser, the corresponding values were $FWHM_x$ = 0.65 ± 0.02 µm, $FWHM_y$ = 0.63 ± 0.01 µm, and $FWHM_z$ = 3.13 ± 0.07 µm (SEM, n = 3 beads). Both laser beams thus resulted in comparable PSFs of approximately $(0.67\ \mu m)^2$ x 3.1 µm focal volume.

### *3.3 The mode-locked semiconductor disk laser*

We designed a prototype mode-locked semiconductor disk laser based on recent improvements in the technology [42]. We used the same gain chip and combined it with a quantum well (QW) SESAM similar to the one used in [42]. A QW SESAM has the advantage of having a faster recovery time compared to quantum dot SESAMs used previously for a SDL developed for MPM [42]. We optimized the laser cavity (depicted in Fig. 2(A)) for long-term stability and ensured operation at room temperature by placing the whole cavity and pump optics in a laser head with a small footprint of 22 cm x 25 cm. The SDL chip was cooled to 16°C and the SESAM was kept at a temperature of 20°C in order to avoid any water condensation in a laboratory environment. Turn-key operation with long-term stability was obtained with strain-compensated semiconductor growth [55].

As presented in Fig. 4, the SDL generated stable and clean mode-locking at a center wavelength of 1027 nm with 9.5 nm of full width at half maximum (FWHM) spectrum supporting 118-fs pulses (measured with a HP-70952B Optical Spectrum Analyzer). The center wavelength was chosen as the recent development of <100 fs SDLs was achieved around 1 µm. Furthermore, this wavelength allows excitation of red fluorescent proteins. The radio frequency (RF) signal was measured with a fast photodiode (Newport 1454, 25 GHz bandwidth) and a radio-frequency spectrum analyzer HP-8592L. The pulse duration of the laser was measured after the objective of the microscope system to take into account the dispersion and spectral filtering that could arise in the system. For this measurement we used a 15-mm focal lens (Thorlabs C260TMD-B**)** to capture the divergent beam exiting the 20x objective. Without additional dispersion compensation, pulses of around 169 fs FWHM (using a $sech^2$ fit) were measured with a Femtochrome Research FR-103MN second-harmonic autocorrelator (Fig. 5(A)), which correspond to 1.44x the transform limit. The laser operates at a repetition rate of 1.63 GHz (Figs. 5(C) and (D)) and could deliver up to 145 mW of average output power at a pump power of 15 W provided by a standard commercial 808 nm fiber coupled diode. With the 20x objective, up to 72 mW (i.e. ~50% of transmission) were available for imaging, corresponding to 230 W of peak power. Using the figure of merit (FOM) defined in [25, 44], we could achieve $FOM_{2PM} = P_{avg} \times P_{peak}$ = 16 $W^2$ below the objective, which was sufficient for MPM imaging in a variety of applications (see section 5).

Biomedical Optics EXPRESS

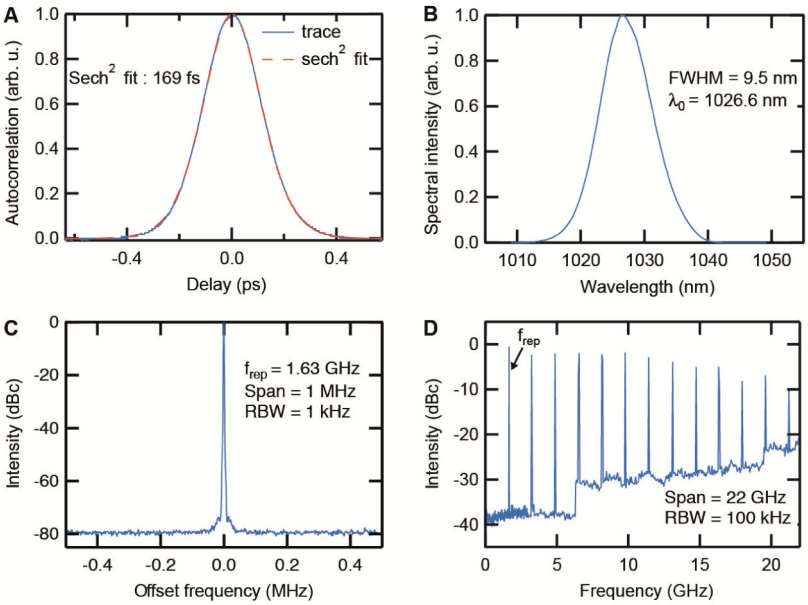


Fig. 5. A) Pulse width measurements of the ultrafast SDL in combination with the 20x microscope objective. B) The SDL has a spectrum with 9.5 nm full width at half maximum (FWHM) (i.e the spectrum is supporting 118 fs pulses). C-D) Fundamental mode-locking is demonstrated with the Radio Frequency (RF) traces taken at the main laser frequency of 1.63 GHz and on its harmonics. The drop of the power in the harmonics is due to the limited bandwidth of the RF amplifier used to measure it. The resolution bandwidth (RBW) is the smallest frequency increment that can be resolved.

As shown in Fig. 2(A), the laser cavity contains only three components in addition to the optical pump, which in combination with the GHz repetition rate leads to a highly compact, stable, and simple laser head.

During the last decade we have observed significant industrial developments of III-V semiconductor foundries for applications in machining, telecommunication or distance ranging. Thus there are commercial suppliers for providing SDL components at high volume. This combination of simplicity and availability of affordable components will support the commercialization of ultrafast SDLs as compact and cost-efficient sources.

### *3.4 The Ti:Sapphire laser*

In order to compare the SDL to a standard laser used in MPM imaging, we used a tunable Ti:Sapphire laser (Mai Tai HP Deep See, Spectra-Physics), which allowed the evaluation of imaging performance for different repetition rates while keeping the other parameters constant (Fig. 6). With clean mode-locking at a repetition rate of 80.65 MHz, i.e. 20.3 times lower than the SDL, the Ti:Sapphire spectrum could be tuned to match the center wavelength of the SDL (Fig. 6(B), with an OceanOptics USB2000 spectrometer). With nearly 12 nm FWHM, the Ti:Sapphire laser spectrum could however support pulses as short as 104 fs at this wavelength. To equalize the pulse lengths, we used the prechirping unit inside the Ti:Sapphire laser. As shown in Fig. 6(A), the pulse duration of this Ti:Sapphire laser could be adjusted to 169 fs below the microscope objective measured with the autocorrelator. The RF traces, which were measured with a fast photodiode (Alphalas UPD-200-SP, 2 GHz bandwidth) and an RF spectrum analyser (Rohde & Schwarz FSH4), indicate fundamental mode-locking (Figs. 6(C) and (D)). Hence, pulse duration, center wavelength and spatial resolution were matched for both lasers with only the repetition rate being different.

Biomedical Optics EXPRESS

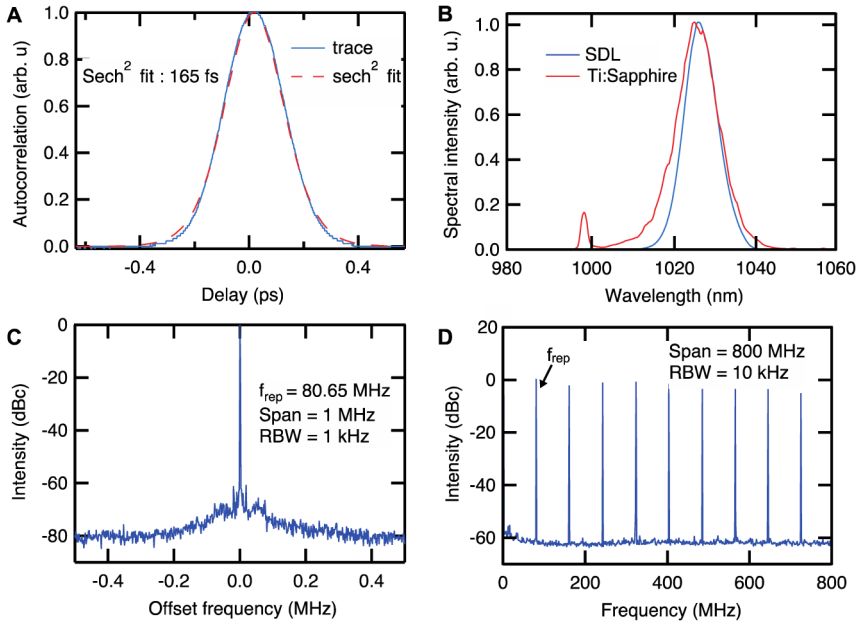


Fig. 6. A Ti:Sapphire laser (Mai-Tai HP from Spectra-Physics) was used for comparison with the SDL. A) Using the prechirping unit in the Ti:Sapphire laser, the pulses were adjusted to a length of 165 fs after the objective (20x). B) The spectrum was centered at 1026 nm to overlap with the spectrum of the SDL. Both spectra were measured after the microscope objective. C-D) Fundamental mode-locking was confirmed by the Radio Frequency (RF) traces taken at the main laser frequency of 80.65 MHz and on its harmonics. The resolution bandwidth (RBW) is the smallest frequency increment that can be resolved.

## 4. Comparison of the SDL and a matched Ti:Sapphire laser

In this section, we evaluate the achievable multiphoton signal levels and bleaching properties of imaging using the SDL in comparison to a standard Ti:Sapphire laser with matched operation parameters except for the different repetition rate (see Section 3 for more details).

### *4.1. Comparison of the generated two-photon signal*

To compare both laser systems we imaged a confocal test slide (FluoCells #2 Molecular Probes), which contains fixed bovine pulmonary artery endothelial cells (BPAEC). In this sample, Texas Red-X phalloidin is labeling F-actin and microtubules are labeled with antibodies conjugated to BODIPY FL. We set the Ti-Sapphire laser to an average power of 11 mW after the 20x objective and imaged the cells by taking a stack of 10 planes at 1 µm spacing (2048 x 2048 pixel images with 10 µs pixel dwell time, 42 s/image). We then set the SDL power to 49 mW, which corresponds to a power ratio of $4.5 \approx 20.3^{1/2} \approx \left( f_{rep,SDL} / f_{rep,Ti-sapphire} \right)^{1/2}$, so that both lasers should produce similar signal levels [3]. Figure 7 shows a comparison of both data sets in the form of a sum projection of all slices and line profiles. The signal levels and resolved features were indeed comparable (a 11-17% difference in generated fluorescence signal can be noted for the SDL), validating the theoretical predictions [3] and the matching of the two laser systems (section 3). The small difference is likely caused by slight inaccuracies in the matching parameters, for example in the pulse duration, or might be due to slight bleaching when sequentially imaging the same volume of the sample with both lasers.

Biomedical Optics EXPRESS

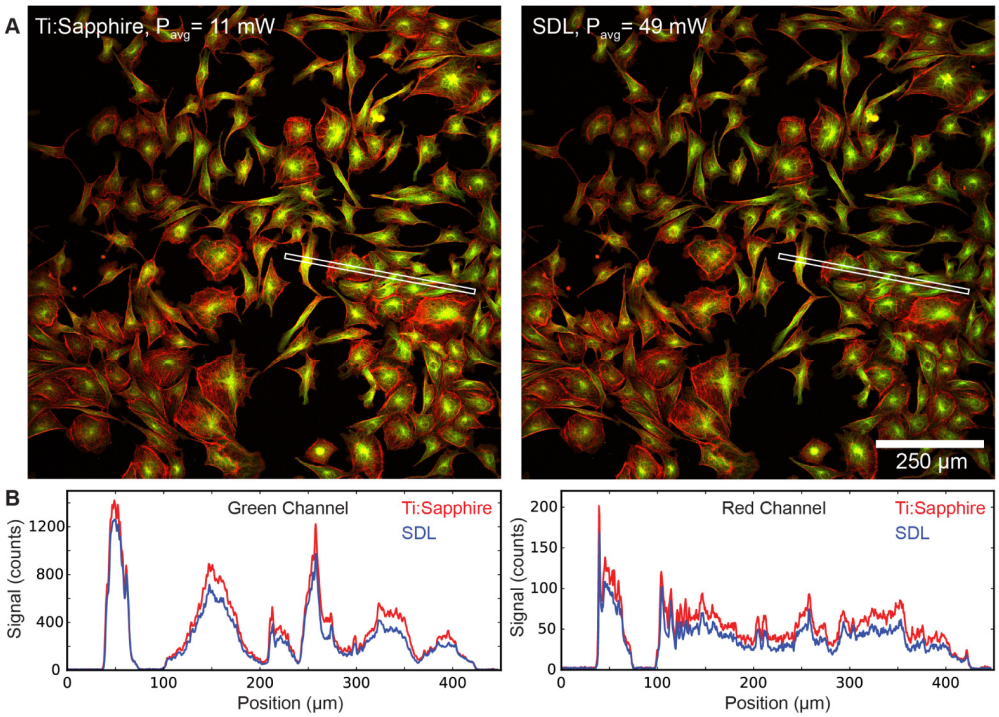


Fig. 7. Imaging comparison between the SDL and the Ti:Sapphire laser: The power levels were set to a ratio of ≈4.5 to create approximately the same signal based on the ratio of repetition rates [48]. The images are sum projections over a stack of 10 slices (taken at 2048 x 2048 pixel with 10 µs pixel dwell time) using 1 µm z-spacing. A) Comparison images of fixed BPAE cells (similar histogram settings). Green channel: Microtubules, red channel: F-Actin. B) Comparison of the signal counts created by the SDL and the Ti:Sapphire laser along the line profiles highlighted in A.

### *4.2. Bleaching comparison*

To investigate the bleaching properties when using the two matched laser systems in our microscope, we performed bleaching tests on a *Drosophila* larva generated by crossing the line UAS-palmKate2-K7 (attP2), driving palmitoylated mKate2 in muscle cells with c381Gal4w + and 332.3Gal4w + [56]. The larva was embedded in Mowiol (Sigma-Aldrich) and regions sized 80.8 x 5.4 µm$^2$ at a depth of 60 µm were imaged at 256 x 16 pixel with 10 µs pixel dwell time over 100 seconds at a frame rate of 15 Hz. The average powers of the Ti:Sapphire laser and the SDL were set to create similar signal counts (14.4 mW and 66.5 mW below the objective, respectively; corresponding to a ratio of ≈4.6). For each laser, the bleaching tests were repeated 4 times (Fig. 8(A)). The bleaching traces observed with the SDL did not exhibit any signs of damage processes related to the higher average power level compared to the Ti:Sapphire laser.

To properly fit the time-dependent fluorescence signal during bleaching, a tri-exponential function was necessary (Figs. 8(A) and (B)) indicating that at least three different bleaching processes with separate dynamics are involved. Simpler fitting functions such as a single- and bi-exponential fit exhibit oscillatory behavior when comparing the residues on normalized traces (Fig. 8(D)).

The time constants ($\tau_1$, $\tau_2$ and $\tau_3$) extracted from the fits then allowed us to calculate the coefficient of photo-damage (β, Fig. 8(D)) using the same approach as in [48]. At $\beta = 2.1 \pm 0.51$, the difference of the SDL and the Ti:Sapphire was very slight, corresponding to a 10-15% improvement in the bleaching rates, which is lower than previously reported values [48].

Biomedical Optics EXPRESS

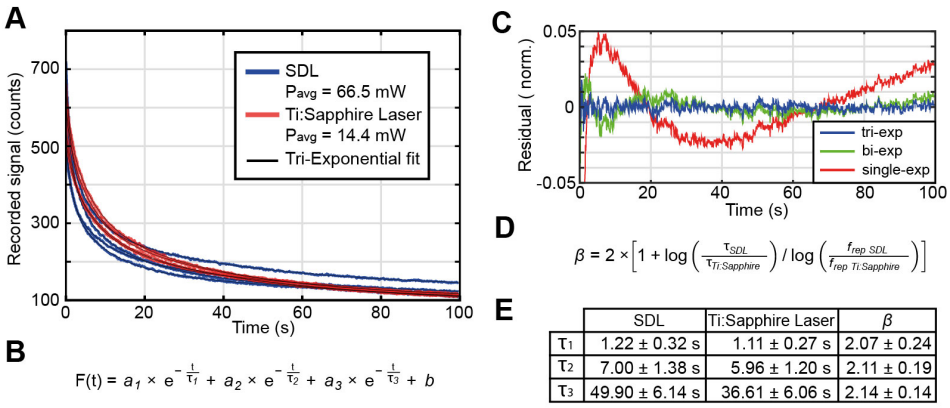


E

| | SDL | Ti:Sapphire Laser | $\beta$ |
|---|---|---|---|
| $\tau_1$ | 1.22 ± 0.32 s | 1.11 ± 0.27 s | 2.07 ± 0.24 |
| $\tau_2$ | 7.00 ± 1.38 s | 5.96 ± 1.20 s | 2.11 ± 0.19 |
| $\tau_3$ | 49.90 ± 6.14 s | 36.61 ± 6.06 s | 2.14 ± 0.14 |

Fig. 8. Comparison of bleaching rates in a *Drosophila* larva labeled with mKate2: A) Raw bleaching time courses for the SDL (blue) and for the Ti:Sapphire laser (red) at a power ratio of 4.6 giving a similar generated signal as expected by theory. B) Tri-exponential function used to fit bleaching curves in A. As shown in C), this function was the most adequate to obtain an accurate and robust fit because a single or bi-exponential function cannot fully fit the data. D) Formula to calculate the photodamage coefficient $\beta$ using the approach in [48]. E) Taking into account the three time constants of the bleaching curves ($\tau_1$, $\tau_2$ and $\tau_3$), $\beta$ can be obtained in each case. The average $\beta$ value across all three extracted time constants is centered at 2.10 with a standard deviation of 0.51.

## 5. In vivo multiphoton imaging using the SDL

In this section we demonstrate the multiphoton imaging capabilities of the SDL for routine *in vivo* imaging experiments in developmental biology and neuroscience. All images shown in this section were acquired with the ultrafast SDL.

### *5.1. In vivo multiphoton imaging in Drosophila*

To demonstrate the compatibility of the SDL with MPM in living organisms, we imaged a Drosophila larva labeled with mKate2 in muscle cells (same line as described in section 4.2). A 3rd instar larva was selected for imaging, dissected and placed in a custom imaging chamber with calcium-free HL3 buffer to reduce motion artifacts. The excited fluorescence signal above 552 nm was collected together with the forward-directed SHG signal by the transmission detection system. A strong red fluorescence signal from muscle cells, together with SHG generated by sarcomeres was detected down to a depth of several hundred microns (Fig. 9, supplementary Visualization 1). The SDL thus provides high enough peak power to generate sufficient two-photon excited fluorescence and SHG signal levels for imaging in small organisms. In fact, the average power levels needed in this experiment (i.e., 17 mW and 6 mW in Fig. 9) were so low that we reasoned that the SDL should be capable of allowing multiphoton imaging under more challenging conditions, for example in samples with higher levels of scattering or using other fluorophores.

Biomedical Optics EXPRESS

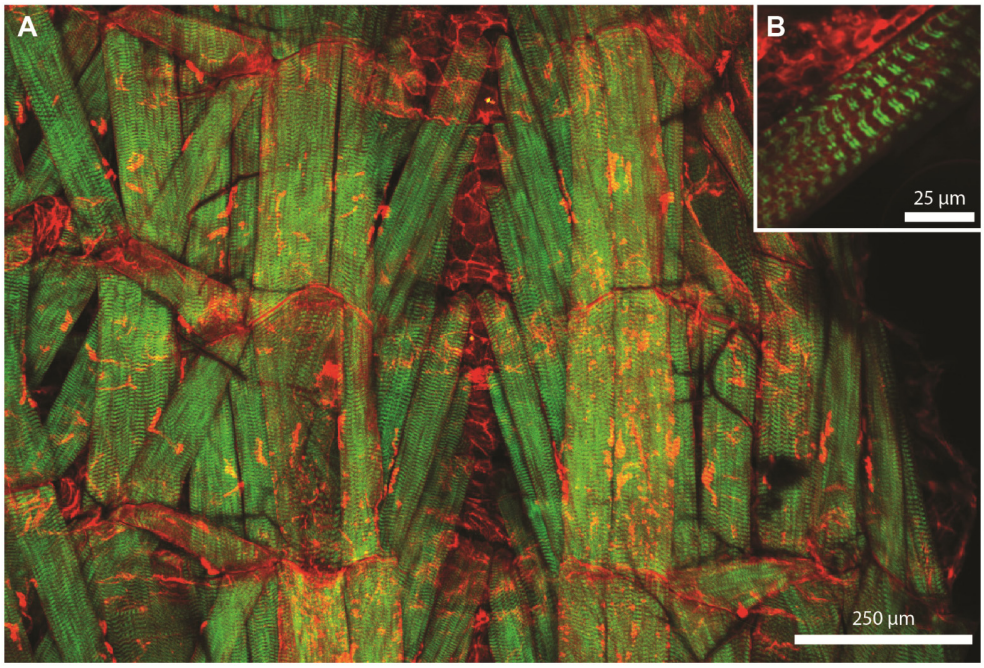


Fig. 9. A) Multiphoton imaging in a *Drosophila* larva using the ultrafast SDL: Maximum intensity projection of a stack covering a range of 160 µm (Average laser power: 17 mW, 1696 x 1142 pixel, 10 µs dwell time). Red channel: Fluorescence from mKate2, Green channel: SHG signal. The SHG signal is predominantly originating from sarcomeres in the muscles. B) Image of the sarcomeres at higher zoom showing the characteristic double-band structure (6 mW, 1024 x 1024 pixel, 10 µs dwell time, 4x averaging).

### *5.2. In vivo two-photon imaging of mouse vasculature in the neocortex*

We then tested the imaging capabilities of the SDL for structural imaging in the living mouse brain. We prepared a chronic cranial window in a C57BL/6 mouse and injected Texas Red conjugated to a high molecular weight dextran (70K MW, Invitrogen) into the tail vein to label the blood plasma. This type of experiment is routinely used to study the structure and function of the brain vasculature, for example to evaluate the coupling between neuronal activity and associated changes in blood flow (neurovascular coupling) [57]. During isoflurane anesthesia, the tail vein was dilated by heating in warm water. The end of the tail was softly clamped and a bolus of dye-containing solution (0.1 ml at 5% wt/vol) was slowly injected. For *in vivo* imaging sessions, isoflurane anesthesia was maintained and the animal's body temperature was kept steady at 36°C. Using the 16x objective and 60 mW of SDL average power, we were able to acquire two-photon images of blood vessels and fine capillaries down to 400 µm depth (Fig. 10, supplementary Visualization 2). At 10-30 µm depth, we also detected the SHG signal created by the collagen-rich dura mater just below the cranial window. All animal procedures were carried out according to the guidelines of the Center for Laboratory Animals of the University of Zurich and were approved by the Cantonal Veterinary Office. This experiment demonstrates that *in vivo* imaging with the SDL is feasible in the superficial layers of the mouse brain despite the lower average power output compared to Ti:Sapphire lasers. The SDL should thus also be applicable for measurements studying the dynamics of blood flow by line scans across single blood vessels [57] and for structural imaging at comparable depths.

Biomedical Optics EXPRESS

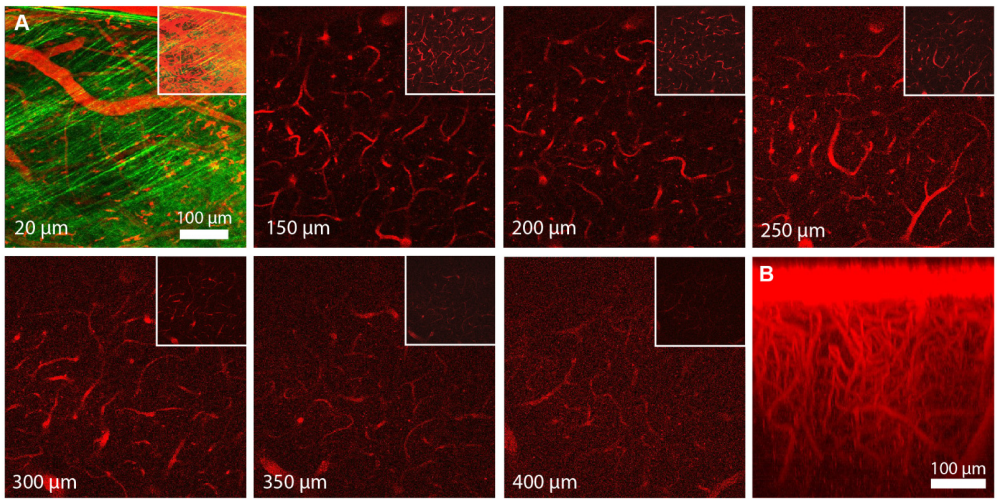


Fig. 10. In vivo two-photon imaging of blood vessels filled with Texas Red Dextran using the ultrafast SDL. A) Selected frames from a z-stack at different depths as measured from the brain surface (512 x 512 pixel, 10 µs pixel dwell time). For each z-plane, the histogram was adjusted for better visibility. The top right insets show the same z-positions with the identical histogram settings throughout to compare signal strength. The SHG signal from the dura mater is visible at 20 µm. B) YZ-side-projection of the same data set (red channel only).

### *5.3. In vivo two-photon imaging of neuronal activity in mice*

A key application of two-photon microscopy in modern neuroscience is functional imaging of the activity of neuronal populations in a living brain through cranial windows. For such recordings across tens to thousands of neurons, fluorophores reporting changes in intracellular calcium concentration are commonly employed [58]. As the center wavelength of the SDL at 1027 nm predominantly allows excitation of red fluorophores, we used the red-shifted genetically encoded calcium indicator R-CaMP1.07 [57], which is efficiently two-photon excited by lasers operating in the range of 1020-1100 nm.

We expressed R-CaMP1.07 in neurons of the mouse brain by using several intracortical stereotaxic injections of an adeno-associated viral serotype 1 (AAV1) vector driving expression under the control of the unspecific EF-α1 promoter (AAV1-EFα1-R-CaMP1.07). For each injection site, 200 nl of virus were injected through glass micropipettes in a C57BL/6 mouse under isoflurane anesthesia in the superficial layers of the somatosensory barrel cortex (100-800 µm depth). After recovery, a cranial window (d = 4 mm) was implanted and *in vivo* imaging recordings were started 10 days post-operation.

Using the 20x objective, we were able to visualize R-CaMP1.07-expressing neurons down to a depth of 360 µm with the SDL (Fig. 11(A)). At a depth of 125 µm, we recorded functional signals at a frame rate of 10.68 Hz on a field-of-view (FOV) of 120 µm x 120 µm which allowed us to resolve calcium transients from a set of neurons (Fig. 11(B), supplementary Visualization 3 and Visualization 4). For plotting neuronal ΔF/F signals, imaging frames were registered to correct for motion artifacts using the template matching and slice alignment plugin in Fiji [59] and regions of interest around cell bodies were selected manually. The SDL allowed recordings of neuronal activity at signal to noise levels comparable to recordings obtained with Ti:Sapphire lasers [60]. These results demonstrate that two-photon calcium imaging in the superficial layers of mouse neocortex at 100-350 µm depths, which is a major type of experiments in current neuroscience, is feasible with an ultrafast SDL.

Biomedical Optics EXPRESS

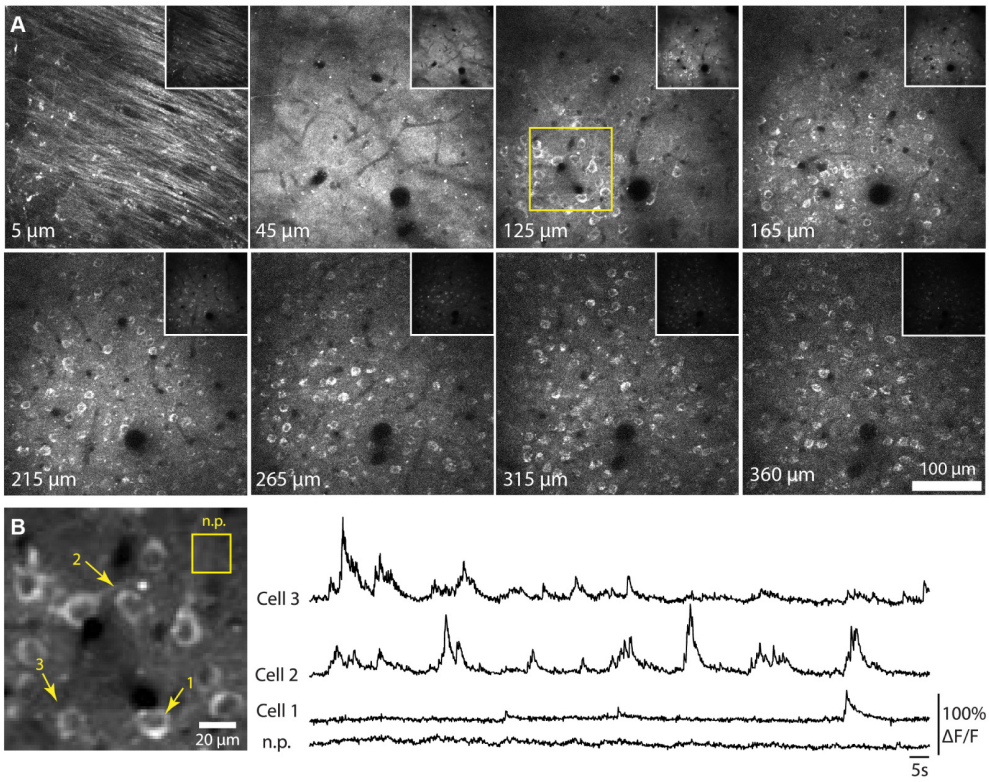


Fig. 11. *In vivo* imaging of R-CaMP1.07-expressing neurons in mouse neocortex using the ultrafast SDL. A) Single z-planes from a stack starting at the dura down to a depth of 360 µm (72 mW laser power, 1024 x 1042 pixel, 10 µs dwelltime). For each z-plane, the histogram was adapted for better visibility. The insets show the same z-positions with the same histogram settings. Neurons are visible as hollow rings as the calcium indicator does not enter the cell nucleus. The yellow frame at a depth of 125 µm indicates the functional imaging region in B). B) Calcium imaging in a subset of neurons (acquired at 72 mW laser power, 100 x 100 pixel, 6 µs dwelltime). Average projection and example traces of three neurons and a neuropil (n.p.) region of interest are shown with a frame rate of 10.68 Hz. For this experiment, an HPD recorded all available signal without additional filters except an IR rejection filter.

### *5.4. In vivo two-photon imaging of neuronal activity in mice with OGB-1*

Finally, we examined whether despite of the long wavelength of 1027 nm of our ultrafast SDL, calcium imaging with indicators normally excited in the 800-900 nm region is feasible as well. For this purpose, we used a VIP-tdTomato mouse, in which inhibitory interneurons expressing vasointestinal polypeptide (VIP) co-express the red marker protein tdTomato.

A postnatal day 8 (P8) mouse was sedated by chlorprothixene (0.1 g/kg, intraperitoneal (i.p.); Sigma-Aldrich Chemie GmbH, Buchs, Switzerland) and lightly anesthetized with urethane (0.25-0.5 g/kg, i.p.). A custom-built head plate was glued to the skull over the left brain hemisphere with dental cement (Paladur, Heraeus Kulzer GmbH) to secure and stabilize the animal. A small cranial window of 1.5 × 1.5 $mm^2$ was opened above the cortical barrel map (guided via intrinsic imaging) with a sharp razor blade and neuronal ensembles in the superficial layers were bolus-loaded with the AM-ester form of Oregon Green BAPTA-1 by pressure injection (OGB-1; 1 mM solution in calcium-free Ringer'solution; 2-min injection at 150-200 µm depth [61]). The craniotomy was filled with agarose (Type III-A, 1% in Ringer's solution; Sigma) and covered with a glass plate.

Biomedical Optics EXPRESS

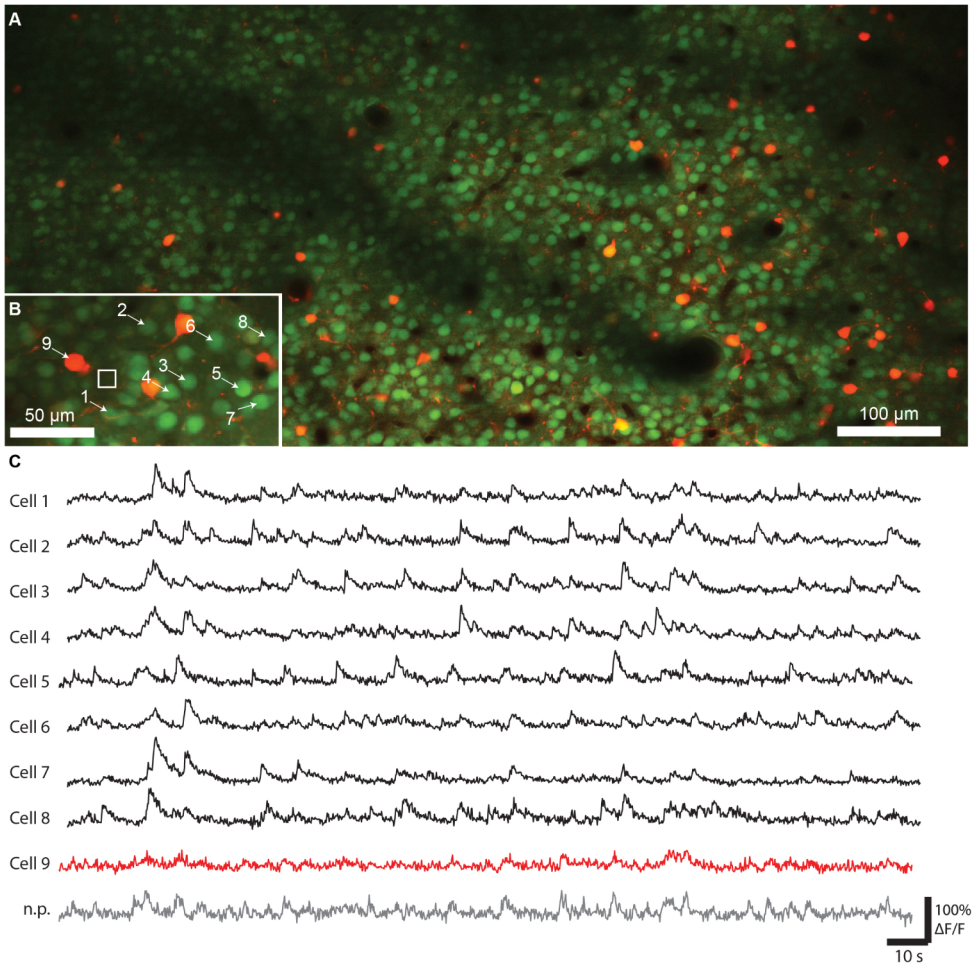


Fig. 12. *In vivo* calcium imaging in a young (P8) mouse with the ultrafast SDL: A) Overview image (924 µm x 465 µm) of tdTomato-expressing VIP-positive interneurons (red) and the surrounding cell population labeled with the calcium indicator OGB-1 (green) at a depth of 140 µm (51.4 mW average power, 3492 x 1598 pixel, 10 µs pixel dwelltime, 4x average). Shadows in the image originate from superficial blood vessels. B) Field-of-view selected for calcium imaging (164 µm x 89 µm, 155 µm depth, 55.8 mW laser power, 200 x 100 pixel, 5 µs pixel dwell time) and calcium transients recorded from several neurons (6.42 Hz frame rate). Cell 9 is a VIP-positive interneuron co-labeled with tdTomato. n.p.: Neuropil.

Using the SDL and the 16x objective, we could efficiently excite tdTomato and OGB-1 and record both large-FOV structural images (Fig. 12(A)) and functional calcium signals (Fig. 12(B)).

For functional recordings, we selected a smaller FOV and detected calcium transients from putative excitatory neurons, astrocytes as well as dual-labelled VIP-positive interneurons (Fig. 12(B), supplementary Visualization 5). The neuronal populations displayed a highly synchronized activity pattern, which is typical for the maturing neocortex in this early postnatal period [62]. Our prototype ultrafast SDL is thus suitable for imaging of a wide range of fluorophores, even though a SDL tailored towards green fluorophores by lowering the laser wavelength would certainly be better suited for such imaging applications.

Biomedical Optics EXPRESS

## 6. Conclusions

We have demonstrated the utility of a femtosecond semiconductor disk laser (SDL) for a broad selection of multiphoton imaging applications, ranging from two-photon excited fluorescence to second harmonic generation in *Drosophila* and mice. In all of our experiments, the ultrafast SDL provided sufficient signal levels to make this laser an attractive alternative to a standard Ti:Sapphire laser for a wide range of experiments in developmental biology and neuroscience.

As predicted by theory [3], imaging of the same sample with a SDL and a Ti:Sapphire laser with matched parameters (pulse duration, center wavelength, and spatial resolution) resulted in comparable signal levels when the SDL average power was appropriately scaled (ratio ≈4.5). In this work, the power levels provided by the laser at 1027 nm were sufficient to image a variety of red fluorophores but also the green calcium indicator OGB-1 (which is typically excited at 800 or 920 nm). Images were obtained from a depth of hundreds of microns in scattering tissue *in vivo*, highlighting that for many imaging applications the complexity and cost of a Ti:Sapphire laser are not necessary. In our SDL experiments, we did not observe heating-induced damage of the samples (due to linear absorption), which could have occurred due to the higher average power compared to the Ti:Sapphire laser. In addition, we stayed far below the threshold for long-lasting damage of brain tissue of 250 mW that has been recently reported [47].

While [48] would predict a two-fold improvement in bleaching rate when using a 20x higher repetition rate, we could not confirm this prediction experimentally. We could nonetheless confirm that the 4.5-fold increased SDL average power did not cause increased photodamage compared to the Ti:Sapphire laser. The absence of an effect of the repetition rate on bleaching may also be caused by differences in samples and fluorophores.

The ultrafast SDL produced equally good imaging results as a Ti:Sapphire laser with similar operation parameters except repetition rate and power even though the two-photon figure of merit [25] of the SDL is lower than the FOM for a Ti:Sapphire laser. The reason is that in the majority of biological imaging experiments, the maximum FOM of the laser is not even close to be utilized due to onset of tissue damage and the high absorption cross section of modern fluorophores.

Whereas the current generation of ultrafast SDLs is not suitable for very deep multiphoton imaging as performed with high-peak-power sources, a cost-efficient and reliable ultrafast source at GHz repetition rates could also be interesting for implementing frequency-type two-photon fluorescence lifetime imaging (FLIM) approaches or to improve photon statistics for fast scanning techniques with pixel dwell times in the <100 ns domain such as low-power temporal oversampling (LOTUS [63]).

While the SDL presented here excites a green fluorophore (OGB-1) with reasonable efficiency, future SDLs will be bandgap-engineered towards center wavelengths in the 750-970 nm region, thus allowing to make full use of the wide range of fluorescent markers currently imaged using Ti:Sapphire lasers.

In summary, we have demonstrated that the current generation of ultrafast SDLs can be successfully used for nonlinear imaging applications. The SDL can thus fulfill the need for a simple, small, and reliable MPM laser source covering a wide range of applications. It will be especially attractive for configuring or upgrading a confocal microscope with multiphoton capabilities at low cost.

## Funding

Swiss Confederation Program Nano-Tera.ch (under the program MIXSEL 2); Swiss National Science Foundation (SNSF); Swiss National Science Foundation (31003A_149858; F.H.); US NIH BRAIN Initiative (1U01NS090475-01, F.H).

Biomedical Optics EXPRESS

## Acknowledgements

The authors acknowledge support of the technology and clean room facility FIRST of ETH Zurich for advanced micro- and nanotechnology. We would like to thank Jade Glashauser for generating *Drosophila* lines and Erich Frei, Marisa Oliveira, Oliver Urwyler, Sebastian Sydlik, and Martin Müller (IMLS, UZH) for providing larvae. Additionally, we would like to thank Justine Kusch-Wieser, Gabor Csucs (Scope-M, ETH Zurich), José María Mateos Melero, and Urs Ziegler (Center for Microscopy and Image Analysis, UZH) for providing test samples and microscope objectives, and Pablo Rivera Fuentes for helpful discussions. Furthermore, we would like to thank Mario Mangold for help during the early stages of this project.

## Disclosure

The authors declare that there are no conflicts of interest related to this article.